Large tensions in random elastic networks

Siu-kau Chan and J. Machta*
Department of Physics and Astronomy, University of Massachusetts, Amherst, Massachusetts 01003
(Received 26 July 1993)

The probability density of large tensions in a random spring network is shown to behave asymptotically as $\rho(T)\sim\exp(-AT^{1/\alpha})$. This result follows from the assumption that large tensions are found at the center of funnel-shaped defects. The probability of finding a defect of a given size then controls the distribution of large tensions. The exponent α $(0<\alpha\leq 1)$ is determined analytically by solving the biharmonic equation for a critical defect. Numerical simulations of random elastic networks are consistent with the analytic results and show explicitly that the largest tensions are found in funnel-shaped defects.

I. INTRODUCTION

Mechanical failure of disordered materials is initiated in regions of high stress so it is of great practical importance to understand the distribution of stresses in random elastic systems. In recent years several simple models have been introduced to study electrical and mechanical breakdown in disordered systems.[1-3] Beale and Srolovitz,[3] extending the random fuse model[1] to elastic systems, considered a random triangular spring network with a critical strain above which each spring irreversibly breaks. As the network is stretched, breakdown first occurs at the spring carrying the largest tension. The distribution of large tensions thus plays a central role in understanding breakdown in this model.

In this paper, we study random triangular networks composed of linear, central-force springs with two spring constants, 1 and K, with $0<K<1$. The fraction of stiff springs is p and we consider values of p away from the percolation threshold. Each spring has a natural length of unity. A small uniform tensile strain is applied at the ends of the network. This paper addresses the following question: Given a random elastic network, what is the probability density for large tensions occurring in a bond? Determining this distribution leads to an interesting theoretical problem combining classical elasticity theory and the statistics of rare events.

The random resistor network is the scalar version of the random spring network and the present study is based on methods previously developed for resistor networks.[4-6] A random resistor network consists of a lattice with a fraction p of resistors having conductance 1 and a fraction $(1-p)$ having conductance G with $0\leq G<1$. The key idea in analyzing both the spring network and resistor network is that the distribution of large stresses (currents) is dominated by rare regions in which the springs (resistors) happen to be configured to concentrate stress (current) in a given bond. Such regions are referred to as critical defects and are analyzed by continuum methods.

For finite-size networks, the expected largest stress (current) is controlled by the expected largest defect in the network. For resistor networks,[4,5] the expected largest current in the network, $\langle i_{\max}\rangle$, increases with the size of the network L, as

$$\langle i_{\max}\rangle\sim i_{\rm ave}(\ln L)^{\alpha}\ , \tag{1.1}$$

where $i_{\rm ave}$ is the average current in the lattice. The exponent α depends on G and the dimension d of the network and is bounded by $0<\alpha\leq 1$. For the case of bond dilution ($G=0$) in $d=2$, Li and Duxbury[4] showed that the critical defect is a line of missing conductors and found

$$\alpha=1\quad(G=0)\ . \tag{1.2}$$

Machta and Guyer,[5] studied the case where all conductors in the network are nonzero and showed that the critical defect is a funnel-shaped region with large conductances in two quadrants and small conductances in the other two quadrants. They find that

$$\alpha=\frac{1-\nu}{d}\quad(0<G<1)\ , \tag{1.3}$$

where ν satisfies

$$\nu=\frac{4}{\pi}\tan^{-1}[G^{1/2}] \tag{1.4}$$

for $d=2$ and,

$$(1-G)P_{\nu}P'_{\nu}+\frac{2}{\pi}(Q_{\nu}P'_{\nu}-GP_{\nu}Q'_{\nu})\cot\left[\frac{\pi\nu}{2}\right]=0 \tag{1.5}$$

for $d=3$ with P_{ν} and Q_{ν} Legendre functions of the first and second kind. Equations (1.4) and (1.5) are obtained by solving Laplace's equation with boundary conditions determined by the funnel-shaped critical defect. Based on these results the asymptotic distribution of currents, $\rho(i)$, in random resistor networks was shown[6] to take the form,

$$\rho(i)\sim\exp(-Ai^{1/\alpha}) \tag{1.6}$$

with α given by Eqs. (1.3)–(1.5). The theoretical prediction, Eq. (1.6), is consistent with numerical simulations[6,7] although it is not possible to reach the true asymptotic large current tail of the distribution. The crossover to the asymptotic form is discussed in Ref. 8.

In this paper, we generalize the approach of Refs. 5

0163-1829/94/49(1)/120(9)/$06.00

and 6 to study the distribution of large tensions in two-dimensional random spring networks (with $0<K<1$) under tensile strain. We argue that the critical defect is again funnel shaped and find that the distribution of large tensions takes the form of Eq. (1.6) with tension replacing current and α determined by eigenvalues of the biharmonic equation rather than Laplace's equation.

The paper is organized as follows. In Sec. II the critical defect is described and analyzed using continuum elasticity theory. In Sec. III the distribution of large stresses is derived from the behavior of critical defects and their probabilities. In Sec. IV we report on a numerical study which confirms several features of the theory. Additional details not covered in this paper may be found in Ref. 9.

II. ANALYSIS OF THE CRITICAL DEFECT USING CONTINUUM ELASTICITY THEORY

The central assumption of this study is that the large tensions in a random elastic network are found in local regions which are most effective in concentrating stress at a single spring. For a given stress, the configuration of springs with the highest probability of occurrence which produces that stress is referred to as a "critical defect". Since the probability of occurrence of a local configuration is determined by the size of the configuration, one can also view the critical defect as the configuration of a fixed size which is most efficient at concentrating stress. Large critical defects occur rarely in random networks but create large tensions and the balance between these opposing trends determines the distribution of large tensions. For large critical defects, continuum mechanics may be used to obtain the relation between the maximum tension in the defect and the size of the defect.

We assume that the critical defect is funnel shaped with stiff springs in the top and bottom regions of the funnel and soft springs in the two side regions as shown in Fig. 1. It is intuitively clear that large stresses are focused through the stiff springs and that the tension will be largest at the central spring in the configuration. For example, this is the principle by which the diamond anvil works. Using continuum mechanics we will determine the optimum opening angle δ for the funnel defect.

It is not obvious that this funnel shape is the most effective shape for its size in concentrating stress. Our justification for this assumption is based on the simpler case of the random resistor network where it is shown analytically[5] that the funnel shape is in fact the critical defect. This conclusion is backed up by numerical studies.[6,7,10] Numerical work presented in Sec. IV supports this picture for the random elastic network. However, in the absence of a proof, our result for α should be interpreted as a lower bound although we believe it is exact.

In the continuum treatment, the defect is a rectangular bimaterial plate divided into sectors, see Fig. 1. Each sector is isotropic and has a finite Young's modulus of either $E_<$ or $E_>$. This defect is embedded in an environment having the sample average Young's modulus. To connect the elastic continuum with the triangular spring network, we note that $K=E_</E_>$ and that the Poisson's ratio P should be constant everywhere in the continuum with $0<P<0.5$. A small coplanar external force is applied through the bus bars, see Fig. 2. The continuum is in static equilibrium in the linear regime. We expect the stress to diverge as a power law near the center of the funnel defect. We seek to determine how the divergence of the stress depends on the opening angle of the funnel δ and the materials parameters.

Planar deformations of the defect are analyzed using the technique of Airy's stress function.[11] The stress function is a solution of the biharmonic equation, $\nabla^4\Phi=0$. Within each sector, the stress function takes the form[12]

$$\Phi=r^{\lambda+1}[A_i\sin(\lambda+1)\theta+B_i\cos(\lambda+1)\theta + C_i\sin(\lambda-1)\theta+D_i\cos(\lambda-1)\theta], \quad (2.1)$$

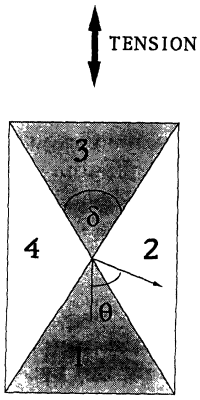

FIG. 1. Analysis of the continuum funnel defect. The origin of the coordinate system is at the center of the defect. The opening angle of the funnel is denoted by δ. The four regions in the defect are labeled to facilitate the discussion.

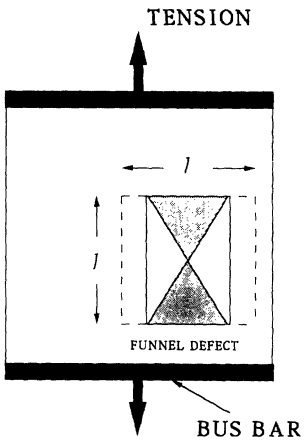

FIG. 2. A two-dimensional elastic network with a funnel defect depicted in it. The Young's modulus of the dark gray region is one, the Young's modulus of the light gray region is K, and the white region has the effective Young's modulus of the full network. The entire network has Poisson's ratio P. One funnel defect is enclosed in a $l\times l$ region. A small force, coplanar with the network, is applied vertically through a pair of horizontal bus bars.

where (r,θ) are polar coordinates as defined in Fig. 1, λ is the eigenvalue to be determined from the analysis and $\{A_i,B_i,C_i,D_i\}$ are constants in the ith sector.

The stress field is obtained from the stress function via[13]

$$\sigma_{\theta\theta}=\frac{\partial^2\Phi}{\partial r^2}\ ,$$
$$\sigma_{rr}=\frac{1}{r}\frac{\partial\Phi}{\partial r}+\frac{1}{r^2}\frac{\partial^2\Phi}{\partial\theta^2}\ , \tag{2.2}$$
$$\sigma_{r\theta}=-\frac{1}{r}\frac{\partial^2\Phi}{\partial r\partial\theta}+\frac{1}{r^2}\frac{\partial\Phi}{\partial\theta}\ ,$$

so that

$$\begin{aligned}\sigma_{rr}=&-\lambda r^{\lambda-1}[A_i(\lambda+1)\sin(\lambda+1)\theta\\&+B_i(\lambda+1)\cos(\lambda+1)\theta\\&+C_i(\lambda-3)\sin(\lambda-1)\theta\\&+D_i(\lambda-3)\cos(\lambda-1)\theta]\ ,\\ \sigma_{\theta\theta}=&\lambda(\lambda+1)r^{\lambda-1}[A_i\sin(\lambda+1)\theta+B_i\cos(\lambda+1)\theta\\&+C_i\sin(\lambda-1)\theta+D_i\cos(\lambda-1)\theta]\ ,\\ \sigma_{r\theta}=&-\lambda r^{\lambda-1}[A_i(\lambda+1)\cos(\lambda+1)\theta\\&-B_i(\lambda+1)\sin(\lambda+1)\theta\\&+C_i(\lambda-1)\cos(\lambda-1)\theta\\&-D_i(\lambda-1)\sin(\lambda-1)\theta]\ ,\end{aligned} \tag{2.3}$$

where $\sigma_{r\theta}$ is shear stress, σ_{rr} and $\sigma_{\theta\theta}$ are normal stress in the r and θ directions, respectively.

Note that the stress field varies as $r^{\lambda-1}$ and diverges at the center of the defect if the real part of the eigenvalue is less than one, i.e., $\mathrm{Re}[\lambda]<1$. On the other hand, the displacement field at the center of the defect must be zero, thus, $\mathrm{Re}[\lambda]>0$.[12] We refer to the smallest eigenvalue (or the λ having the smallest real part if λ is complex) as the dominant eigenvalue. The dominant eigenvalue determines how stress is concentrated at the center of the defect and ultimately controls the tail of the distribution of large tensions in random elastic networks.

The displacement field is derived from the stress function[14] as

$$\frac{\partial u_r}{\partial r}=\frac{1}{2\mu_i}\left[\sigma_{rr}-\left[1-\frac{m}{4}\right]\nabla^2\Phi\right]\ ,$$
$$\frac{\partial u_\theta}{\partial r}-\frac{u_\theta}{r}+\frac{1}{r}\frac{\partial u_r}{\partial\theta}=\frac{1}{\mu_i}\sigma_{r\theta}\ , \tag{2.4}$$

where $m=4/(1+P)$, μ_i is the shear modulus of the ith sector, u_r and u_θ are displacements in the radial and angular directions, respectively. Inserting Eqs. (2.1) and (2.3) into Eq. (2.4) and integrating from the center of the defect, yields the displacement fields,

$$\begin{aligned}u_r=&\frac{r^\lambda}{2\mu_i}[-A_i(\lambda+1)\sin(\lambda+1)\theta\\&-B_i(\lambda+1)\cos(\lambda+1)\theta\\&+C_i(-\lambda-1+m)\sin(\lambda-1)\theta\\&+D_i(-\lambda-1+m)\cos(\lambda-1)\theta]\\ u_\theta=&\frac{r^\lambda}{2\mu_i}[-A_i(\lambda+1)\cos(\lambda+1)\theta\\&+B_i(\lambda+1)\sin(\lambda+1)\theta\\&-C_i(\lambda-1+m)\cos(\lambda-1)\theta\\&+D_i(\lambda-1+m)\sin(\lambda-1)\theta]\ .\end{aligned} \tag{2.5}$$

At the bonding edge of each pair of adjacent sectors, the normal and tangential components of stress and displacement have to match.[14] For instance at the bonding edge at $\theta=\delta/2$,

$$\begin{aligned}\sigma_{\theta\theta}(\theta^-)&=\sigma_{\theta\theta}(\theta^+)\ ,\\ \sigma_{r\theta}(\theta^-)&=\sigma_{r\theta}(\theta^+)\ ,\\ u_\theta(\theta^-)&=u_\theta(\theta^+)\ ,\\ u_r(\theta^-)&=u_r(\theta^+)\ ,\end{aligned} \tag{2.6}$$

where δ is the opening angle of the funnel defect, see Fig. 1. There are 16 such bonding conditions, four at each bonding edge, and there are 16 unknown constants, four from each sector, i.e., $\{A_i,B_i,C_i,D_i$ with $i=1,2,3,4\}$. This system of 16 homogeneous equations of 16 unknowns in matrix form is $\mathbf{Mx}=\mathbf{0}$ and for a nontrivial solution, the determinant of $\mathbf{M}$ must vanish. This constraint yields the compatibility equation which determines λ.

Symmetry about the horizontal and vertical axes of the funnel defect (see Fig. 1) permits one to consider a smaller system of equations. Since there are no shearing stresses or normal displacements along the two axes, i.e., $\sigma_{r\theta}(\theta)=0$ and $u_\theta(\theta)=0$ at $\theta=0°$, 90°, 180°, and 270°, we may study only one-quarter of the defect (i.e., $0°\le\theta\le90°$), which involves only four unknown constants (two from each side of the bonding edge at $\theta=\delta/2$) and four bonding conditions. Therefore, the compatibility equation can be derived from a 4×4 determinant.

The compatibility equation involves four elastic constants (two from each distinct elastic phase, for instance, Young's modulus and Poisson's ratio). However, each sector in the funnel defect is isotropic and the external stress is applied only along the bus bars. Furthermore, the funnel defect is under planar deformation. Thus, the compatibility equation can be written in a much simpler form in terms of two composite (or Dundurs') parameters.[14,15] For this case of equal Poisson's ratio in the two phases, the Dundurs' parameters (a,b) are given by

$$a=\frac{\mu-1}{\mu+1}\,,\qquad b=a\left[1-\frac{2}{m}\right]\,, \tag{2.7}$$

where $m=4/(1+P)$ and the ratio of shear moduli of the two phases $\mu=E_{<}/E_{>}=K$. In terms of the Dundurs' parameters a and b, the compatibility equation (which we derived from the 4×4 determinant with the aid of *Mathematica*[16]) is

$$\begin{aligned}
&-\lambda^3(a-b)^2\frac{\sin^2\delta}{\sin^2(\lambda\pi/2)}+\lambda^2\left\{2ab\sin\delta\left[\frac{\sin\delta}{\sin^2(\lambda\pi/2)}+\sin(\lambda\delta)+\cot(\lambda\pi/2)\cos(\lambda\delta)\right]\right.\\
&\qquad -2(a-b)\cot(\lambda\pi/2)\sin\delta[\cos(\lambda\delta)-\cot(\lambda\pi/2)\sin(\lambda\delta)]-a^2\frac{\sin^2\delta}{\sin^2(\lambda\pi/2)}\\
&\qquad \left.+b^2\sin\delta\left[-\frac{\sin\delta}{\sin^2(\lambda\pi/2)}-2\sin(\lambda\delta)-2\cot(\lambda\pi/2)\cos(\lambda\delta)\right]\right\}\\
&+\lambda\{b^2[(\cos(\lambda\delta)-\cot(\lambda\pi/2)\sin(\lambda\delta))^2-1-2\sin\delta(\sin(\lambda\delta)+\cot(\lambda\pi/2)\cos(\lambda\delta))]\\
&\quad +a^2[\sin(\lambda\delta)+\cot(\lambda\pi/2)\cos(\lambda\delta)]^2+2ab\sin\delta[\sin(\lambda\delta)+\cot(\lambda\pi/2)\cos(\lambda\delta)]\\
&\quad -2(a-b)\cot(\lambda\pi/2)\sin\delta[\cos(\lambda\delta)-\cot(\lambda\pi/2)\sin(\lambda\delta)]-\cot^2(\lambda\pi/2)\}\\
&\qquad +a^2[\sin(\lambda\delta)+\cot(\lambda\pi/2)\cos(\lambda\delta)]^2+b^2[(\cos(\lambda\delta)-\cot(\lambda\pi/2)\sin(\lambda\delta))^2-1]-\cot^2(\lambda\pi/2)=0\,.
\end{aligned} \tag{2.8}$$

We solved for λ numerically at various opening angles for different values of P and K. Figure 3 displays the dominant eigenvalue versus the opening angle for $P=0.4$ and $K=0.1$, 0.5, and 0.9. Notice that the dominant eigenvalues are real at all opening angles. It should be noted that the eigenvalue approaches one, the homogeneous limit, as the opening angle approaches 0° and 180°. Also, the eigenvalue exhibits a minimum at about 60°, i.e., the stress near the center of a funnel defect is largest when δ is about 60°. This largest stress increases as K decreases, i.e., as the difference in strengths of the bimaterial increases. However, the largest stress (or the minimum dominant eigenvalue) is a very weak function of P, see Fig. 4. The largest stress occurs at an angle which depends only on P and increases slowly from approximately 59° as P decreases, see Fig. 5.

A weak dependence of the dominant eigenvalue on Poisson's ratio is also noticed in a previous study on stress singularities at interface corners in bonded dissimilar isotropic elastic materials, see Ref. 18.

One interesting observation is that although the eigenvalues [i.e., the solutions to Eq. (2.8)] are complex in general, the dominant eigenvalue λ (that is, the one which

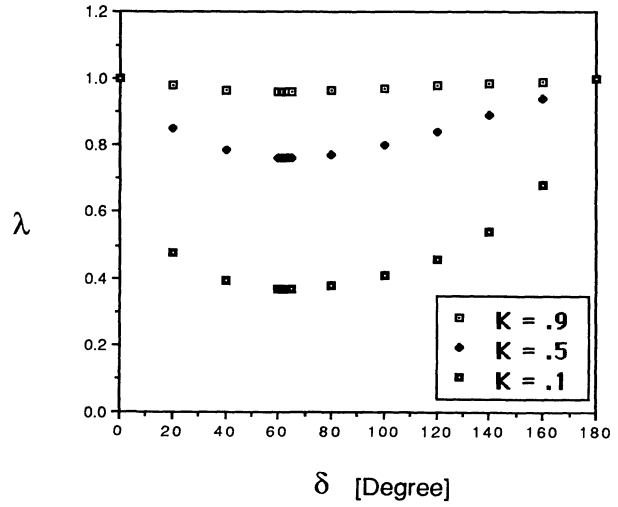

FIG. 3. Dominant eigenvalue versus opening angle. The dominant eigenvalues at various opening angles are plotted for $P=0.4$ and $K=0.1$, 0.5, and 0.9. The eigenvalues exhibit a minimum at an opening angle of about 60°. [For a uniform triangular net, $P=\frac{1}{3}$ (Ref. 17).]

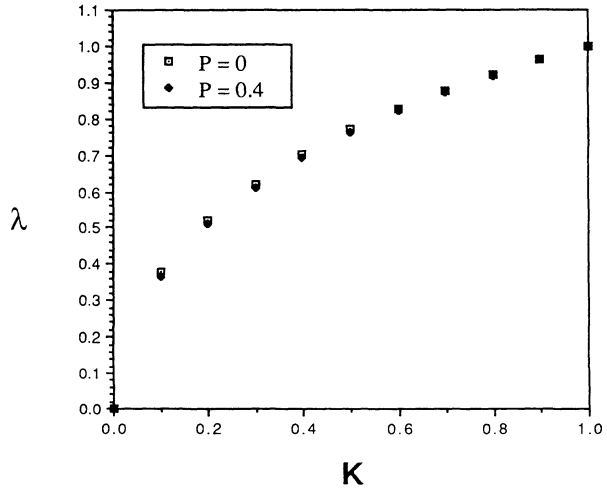

FIG. 4. Dependence of minimum eigenvalue on K and P. The minimum eigenvalue is plotted against the ratio of Young's moduli for two different Poisson's ratios. The dependence on P is much weaker than that on K.

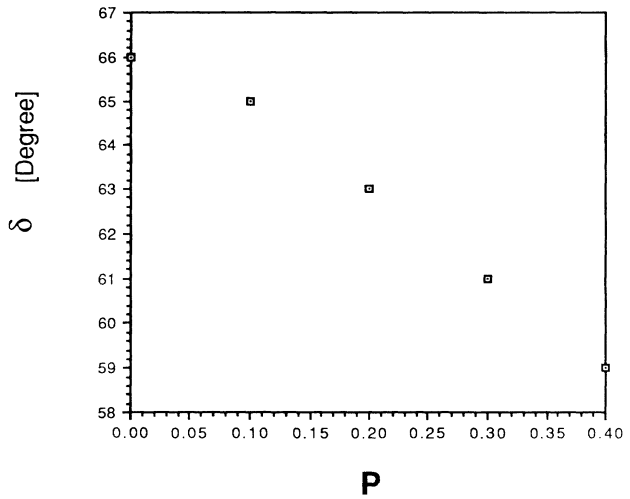

FIG. 5. Dependence of the critical opening angle on Poisson's ratio. The critical opening angle δ is the angle at which the minimum eigenvalue occurs.

has the smallest real part, $0<\mathrm{Re}[\lambda]<1$) is real. On the other hand, all the eigenvalues for the random resistor network, see Eqs. (1.4) and (1.5), are real.

III. PROBABILITY DENSITY FOR LARGE TENSIONS

In this section we obtain the asymptotic behavior of the probability per spring of finding a tension T. The key assumption in this analysis is that a given large tension is almost certainly found in the associated critical defect for that tension. The critical defect is defined as the configuration with the highest probability of occurrence which produces the given tension. In a random network the highest probability of occurrence is associated with the smallest number of specified bonds so we are really asking for the smallest defect capable of producing a given tension. The continuum analysis indicates that the critical defect is funnel shaped with an opening angle of about 60° and that the stress diverges near the center of the defect as $r^{\lambda-1}$. For a spring lattice this divergence is cut off at the length of the spring q. Thus, the estimate for the tension $T(l)$ in the central spring of a funnel defect of size l is

$$T(l)\sim cT_{\mathrm{ave}}\left[\frac{l}{q}\right]^{1-\lambda}, \tag{3.1}$$

where T_{ave} is the average tension in an oblique spring and c is a constant of order unity.

The next ingredient needed for obtaining the distribution of large tensions is the statistics of defect sizes.[6] The probability per unit that an $l\times l\tan(\delta/2)$ region is configured as a funnel with $\delta=60°$ is given by $[p(1-p)]^{l^2/(q^2 2\sqrt{3})}$. This is roughly the probability density $F(l)$ for a given bond to be at the center of a funnel of size l,

$$F(l)\sim e^{-c'l^2} \tag{3.2}$$

with c' a constant.

Assuming that large tensions are almost always found at the center of critical defects, the density of large tensions, $\rho(T)$ is given by the density of defects of size l where the variables are related by Eq. (3.1),

$$\rho(T)dT\approx F(l)dl\ . \tag{3.3}$$

A tension T which is found at the center of a critical defect of size l may also be found in larger regions however the probability of such regions is exponentially smaller [see Eq. (3.2)] and these regions leads to subdominant corrections to the leading behavior of $\rho(T)$. Ignoring subdominant terms and combining Eqs. (3.1)–(3.3) we obtain

$$\ln\rho(T)\sim -A\,(T/T_{\mathrm{ave}})^{1/\alpha} \tag{3.4}$$

with

$$\alpha=\frac{1-\lambda}{2}\ ,$$

$$A\approx -\frac{\ln[p(1-p)]}{2\sqrt{3}}\ ,$$

and λ obtained from Eq. (2.8). Although the above results depend on several unproved assumptions, we believe that both the form of the asymptotic behavior and the value of α given by Eq. (3.4) is exact.

The expected largest tension $\langle T_{\mathrm{max}}\rangle$ in a finite-size network of size L is estimated as the tension whose probability equals the inverse of the number of bonds in the network, thus

$$\langle T_{\mathrm{max}}\rangle\sim T_{\mathrm{ave}}(\ln L)^{\alpha}\ . \tag{3.5}$$

IV. NUMERICAL SIMULATION

In this section, we study the distribution of tensions in a spring network and explore the configuration of springs around the largest tensions using numerical simulations.

We simulated two-dimensional triangular networks of size 99×99 with periodic boundary conditions in the direction transverse to the applied force. We used $p=0.8$ and three values of K; 0.25, 0.5, and 0.75. A small tension (in the linear regime) was applied to the bus bars of each network. We used the method of successive relaxation[19] to compute the equilibrium position for each node. The solution was considered accurate when the magnitude of the total force at each node was below 1×10^{-5}. Using a Cyber 205 supercomputer, relaxation of a network typically took 20 sec.

For each value of K, we computed the tensions in each spring for 50 networks. To avoid edge effects, we excluded the six rows of oblique and the six rows of horizontal bond tensions adjacent to each bus bar in collecting data. With the remaining bond tensions, the probability density of bond tensions was constructed for each value of K. All the bond tensions were normalized with respect to T_{ave}, the average tension in an oblique bond. The probability distributions are displayed in Fig. 6. Note that if $K=1$, the distribution consists of delta functions at $T=0$ and $T=T_{\mathrm{ave}}$, respectively, corresponding to horizontal bonds

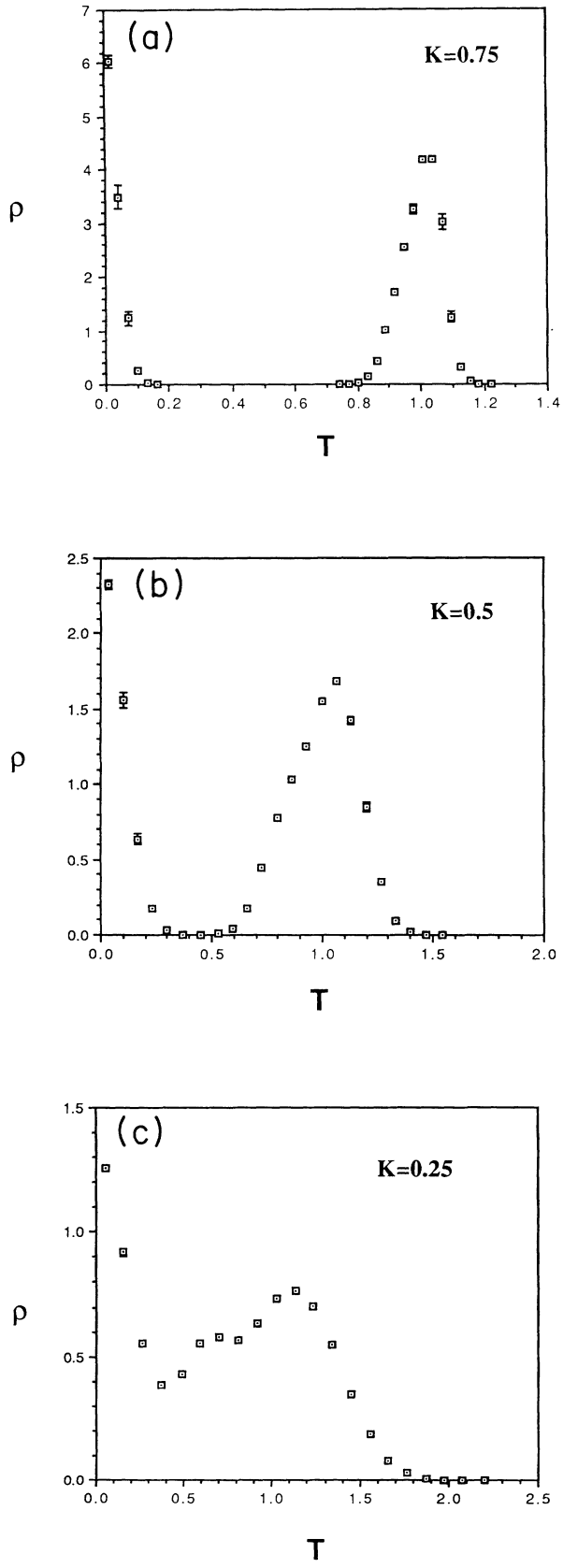

FIG. 6. Distribution of tensions in an ensemble of 50 configurations of 99×99 networks with a given K, where ρ is the density of tensions of magnitude T. (a) $K=0.75$, (b) $K=0.5$, (c) $K=0.25$.

and oblique bonds. As K decreases, the peaks broaden and overlap.

To test the theoretical predictions, we determined an effective value of the exponent α by fitting the tail of the distribution of tensions to the form

$$\ln\rho(T)\sim -A\,(T/T_{\text{ave}})^{1/\alpha}+b \tag{4.1}$$

with A, α, and b as fitting parameters for a least-squares fit. For $K=0.75$, we grouped tensions into uniform intervals of size 0.03 and considered the largest 1.14% of the tensions. For $K=0.5$, we chose an interval size of 0.07 and the largest 0.78% of tensions; for $K=0.25$, we chose interval size of 0.11 and the largest 0.125% of tensions. To display the fit as a straight line, we plotted $\ln[\ln b+\ln(1/\rho)]$ versus $\ln T$ for each value of K in Fig. 7.

In Fig. 8 the effective values of α obtained from the data and the theoretical values of α are plotted versus K. The theoretical values are obtained from Eqs. (2.8 and 3.4) with $\delta=60°$ and $P=0.4$. (The Poisson's ratio for a uniform triangular network[17] is $\frac{1}{3}$, so it might be preferable to have chosen $P=\frac{1}{3}$ for comparison between theory and simulation. However due to the weak dependence on P, this would make almost no difference.)

The effective exponent obtained from the simulations is close to but larger than the theoretical value. We believe that this is because the sampled tensions are not in the asymptotic regime. It is not computationally feasible to probe very large tensions because the distribution decays very rapidly so that an enormous number of samples would be needed to see a small number of large tensions. However, as is the case for the resistor network,[6,8] the effective exponent for relatively small values of α is surprisingly near the theoretical asymptotic value.

In additional to the direct test of the theoretical predictions, we also examined the key assumptions underlying the theory. The first assumption is that the magnitude of the tension in a given spring with a large tension is determined by the configuration of the neighboring springs. To test this assumption, we computed the tension in each spring in the network and found the spring having the largest tension together with its local environment so long as the local environment did not intersect the boundary. The local environment was chosen to be 13×13, see Fig. 9. We performed this study with $K=0.75$. The spring which has the largest tension is slanted either upward and to the left or upward and to the right. The right slanting central bond is marked with a black circle in Fig. 9. Once the large tension was selected, its local environment was cut out from the network. We refer to this local environment as a "hot environment." Next we selected from the rest of the network the smallest oblique bond tension (which is not adjacent to one of the 10 largest tensions). We refer to the local environment of this oblique bond as the "cool environment." We cut out the cool environment and used it to fill the hole in the network left behind by the hot environment. The hole left behind by the cool environment was then filled by the hot environment.

This "cut-and-swap" procedure created a different global environment but maintained a similar local environ-

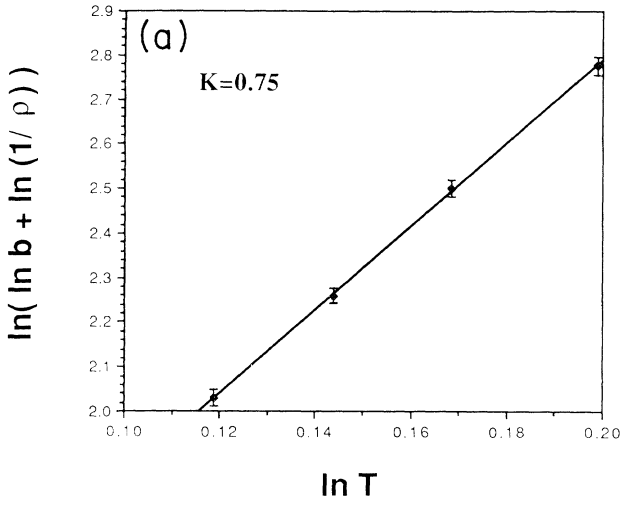

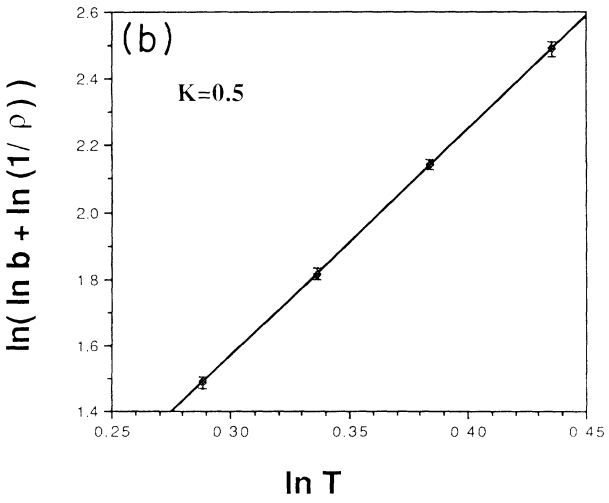

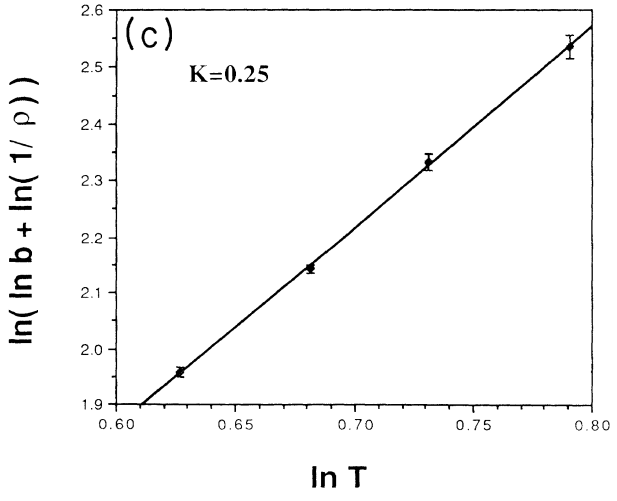

FIG. 7. $\ln[\ln b + \ln(1/\rho)]$ versus $\ln T$ for several values of K. The slope of this plot is equal to $1/\alpha$, see Eq. (4.1). (a) $K=0.75$, (b) $K=0.5$, (c) $K=0.25$.

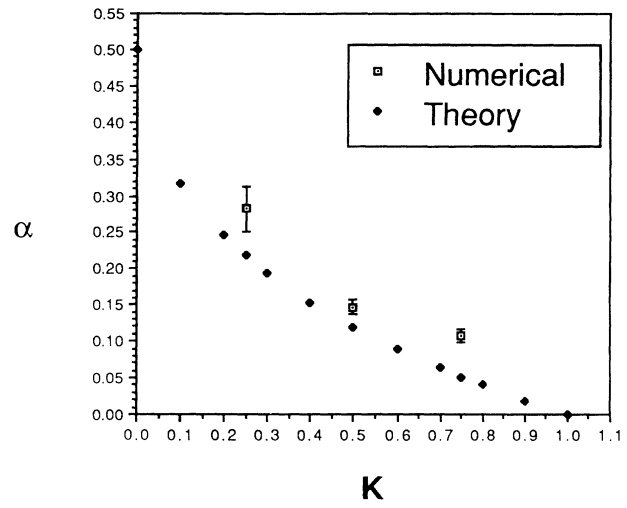

FIG. 8. Comparison of numerical and theoretical results. The theoretical prediction are obtained from Eqs. (2.8) and (3.4) with $P=0.4$. The numerical values of α obtained from Fig. 10 are compared to prediction. The error bars are set by the ranges of slopes in Fig. 10.

ment for the hot bond. We recomputed the tension in this hot bond by recomputing the tension in each spring in the rearranged network and found that the hot bond had virtually the same tension as it did originally. The cut-and-swap procedure was applied five times to the hot environment in the network, each time with a different cool environment from the same network. In this manner, we studied the largest tensions from five different networks and observed a maximum change in tension magnitude of 1.7%. (For comparison, the median of oblique bond tensions is more than 13% below the large tensions studied here.) Having established that it is the local environment which determines the bond tension, we

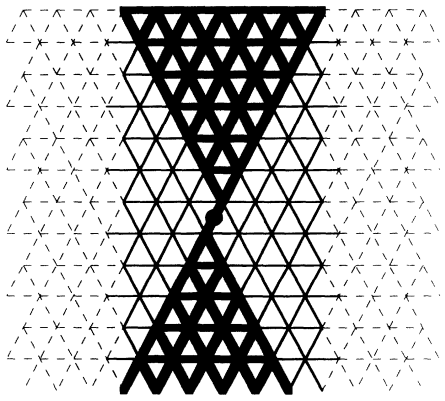

FIG. 9. The funnel defect. The stiff and soft springs in the defect are, respectively, denoted by thick and thin bonds. This defect is embedded in a background, indicated by dotted bonds, of randomly distributed stiff and soft springs. The applied force is in the vertical direction. In this illustration, the largest tension is found at the right slanting bond which is marked with a black circle.

can now study the critical defect in more detail.

We investigated the critical defect by examining the distributions of stiff and soft springs in the neighborhoods of hot bonds. Fifty networks were studied with $K=0.75$. In each network, the local environments of the ten hottest bonds were cut out. Some of these hot bonds slant to the left, while the rest slant to the right. The hot bonds which slant to the left were rotated with their environments about the vertical axis by 180° so that now all hot bonds slant to the right. The hot bond was chosen as the origin of the coordinate system in each hot environment and all of the hot environments were projected onto a two-dimensional plane. For each bond location, we counted the number of hot environments which have a stiff spring at that bond. The fraction of hot environments which have a stiff spring at each bond is displayed in Fig. 10. The *a priori* expected fraction of stiff springs at each bond is equal to p which is 0.8 in this study. An excess of stiff springs at a bond is represented by a black circle at the bond; an excess of soft springs at a bond is represented by a gray circle. A larger circle indicates a greater excess and the absence of a circle indicates values close to 80%. The hot bond is always a stiff spring and is represented by a black square. The funnel shape is roughly apparent in Fig. 10 and the opening angle is observed to be about 60°.

The predicted funnel shape is symmetric about the direction of the average strain but the observed funnel has an asymmetry which we believe is due to the oblique direction of the hot bond. We believe that this is a local effect and would not affect the global shape of the very large defects associated with very large tensions.

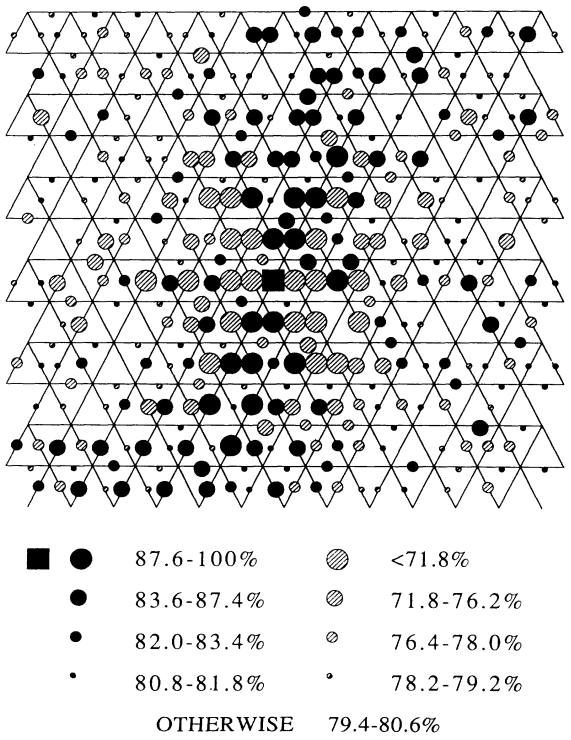

FIG. 10. Funnel defect observed numerically. The distribution of springs in the neighborhood of a hot bond obtained from an average of 500 hot bonds. The largest tension is located at the bond with the black square. The ensemble averaged fraction of stiff springs at each bond is represented by the size of the associated circle as indicated above. The externally applied tension is along the vertical axis.

V. DISCUSSION

We have studied the distribution of large tensions in random spring networks and have shown using both analytic arguments and numerical simulations that the tail of this distribution decays as an exponential of a power. The power law is controlled by an exponent α which is determined by the divergence of stress approaching the center of a funnel-shaped critical defect. We find good agreement between the theory and the simulations.

The "Lifschitz-type" statistical arguments used here depend on the presence of large critical defects. For uncorrelated randomness we are able to estimate the probability of a critical defect of a given size. Although this probability diminishes exponentially with size, it controls the large tensions in the system. Real materials generally display correlated randomness which may lead to modifications of the results found here.

The random spring network under tensile loading and the random resistor network turn out to be very similar systems. The large stresses or currents are controlled in each case by funnel-shaped defects. The difference between the two cases is that the opening angle of the funnel for the resistor case is 90°, while it is close to 60° for the elastic case. The analysis for the elastic case is more mathematically complicated and depends weakly on an additional parameter, the Poisson's ratio. Nonetheless, at the end of the calculations, the values of α as a function of the ratio of spring constants or conductances are surprisingly close to one another. This is illustrated in Fig. 11 where the eigenvalues ν and λ are plotted against G and K, respectively. We do not know whether this quantitative similarity between the two cases is accidental

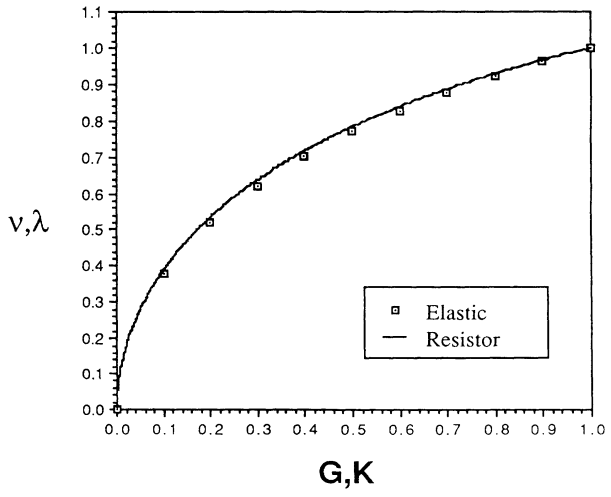

FIG. 11. Comparison of dominant eigenvalues for the resistor network, Eq. (1.4) and spring networks, Eq. (2.8). The eigenvalue for the elastic network is obtained at $P=0$.

or reflects a deeper connection between Laplace's equation and the biharmonic equation. An examination of the three-dimensional case would be of practical value and might shed some light on this question. It would also be interesting to examine the case of shear loading.

We have restricted this study to the linear regime. As one probes further into the tail of the stress distribution, this requires smaller and smaller applied strains since it is not the average stress but the maximum stress which determines whether the system is in the linear regime. Strictly speaking then, the theory applies to the case of infinitesimal strain. It would be interesting to extend these ideas to include nonlinearities.

ACKNOWLEDGMENTS

This work was supported in part by NSF Grants No. DMR 8602705 and 9014366, and by the John von Neumann National Supercomputer Center. One of us (S.C.) would like to thank Tom Lardner for stimulating discussion and pointing out several invaluable references concerning elasticity. We thank Phil Duxbury for useful discussions.

---

*Internet address: machta@phast.umass.edu

[1]L. de Arcangelis, S. Redner, and H. J. Herrmann, J. Phys. Lett. (Paris) **46**, L585 (1985); H. Takayasu, Phys. Rev. Lett. **54**, 1099 (1985).

[2]P. M. Duxbury, P. D. Beale, and P. L. Leath, Phys. Rev. Lett. **57**, 1052 (1986).

[3]P. D. Beale and D. J. Srolovitz, Phys. Rev. B **37**, 5500 (1988).

[4]Y. S. Li and P. M. Duxbury, Phys. Rev. B **36**, 5411 (1987).

[5]J. Machta and R. A. Guyer, Phys. Rev. B **36**, 2142 (1987).

[6]Siu-kau Chan, J. Machta, and R. A. Guyer, Phys. Rev. B **39**, 9236 (1989).

[7]I. Ootani, Y. H. Ohashi, K. Ohashi, and M. Fukuchi, J. Phys. Soc. Jpn. **61**, 1399 (1992).

[8]P. M. Duxbury, R. A. Guyer, and J. Machta (unpublished).

[9]Siu-kau Chan, Ph.D. thesis, University of Massachusetts, 1991.

[10]J. Helsing, J. Axell, and G. Grimvall, Phys. Rev. B **39**, 9231 (1989).

[11]L. D. Landau and E. M. Lifshitz, *Theory of Elasticity* (Pergamon, New York, 1986).

[12]M. L. Williams, J. Appl. Mech. **74**, 526 (1952).

[13]D. S. Dugdale and C. Ruiz, *Elasticity for Engineers* (McGraw-Hill, London, 1971).

[14]D. B. Bogy, J. Appl. Mech. **35**, 460 (1968).

[15]J. Dundurs, J. Appl. Mech. **36**, 650 (1969).

[16]S. Wolfram, *Mathematica* (Addison-Wesley, Reading, MA, 1988).

[17]A. R. Day, K. A. Snyder, E. J. Garboczi, and M. F. Thorpe, J. Mech. Phys. Solids **40**, 1031 (1992).

[18]D. B. Bogy and K. C. Wang, Int. J. Solids Struct. **7**, 993 (1971).

[19]W. Tang and M. F. Thorpe, Phys. Rev. B **37**, 5539 (1988).

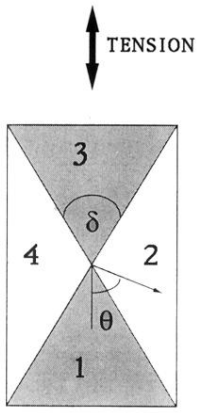

FIG. 1. Analysis of the continuum funnel defect. The origin of the coordinate system is at the center of the defect. The opening angle of the funnel is denoted by δ. The four regions in the defect are labeled to facilitate the discussion.

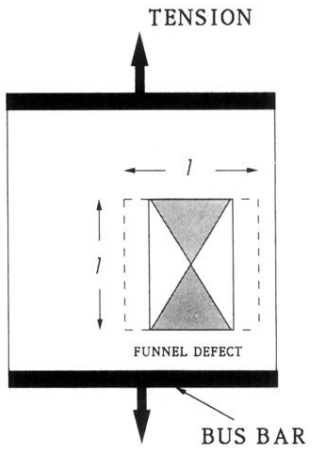

FIG. 2. A two-dimensional elastic network with a funnel defect depicted in it. The Young's modulus of the dark gray region is one, the Young's modulus of the light gray region is K, and the white region has the effective Young's modulus of the full network. The entire network has Poisson's ratio P. One funnel defect is enclosed in a $l \times l$ region. A small force, coplanar with the network, is applied vertically through a pair of horizontal bus bars.